University of Nevada, Reno

Bending Of Metallic Thin Foil Via High Energy Pulsed Laser Peening

A thesis submitted in partial fulfillment of the
requirements for the degree of Master of Science in
Mechanical Engineering

by
Christopher James Yocom

Dr. Yiliang Liao/Thesis Advisor

December 2017

THE GRADUATE SCHOOL

We recommend that the thesis
prepared under our supervision by

CHRISTOPHER JAMES YOCOM

Entitled

Bending Of Metallic Thin Foil Via High Energy Pulsed Laser Peening

be accepted in partial fulfillment of the
requirements for the degree of

MASTER OF SCIENCE

Yiliang Liao, Ph.D., Advisor

Matteo Aureli, Ph.D., Committee Member

Bin Li, Ph.D., Graduate School Representative

David W. Zeh, Ph.D., Dean, Graduate School

December, 2017

ABSTRACT

Laser Peen Forming (LPF), a novel method used to form thin metallic engineering foils, is a manufacturing process utilizing strong shockwaves induced by high pressures introduced to the surface of a target by high energy, pulsed laser beams. It is a non-thermal, non-contact approach that improves the hardness and fatigue life of components by imparting beneficial residual stresses on the surface of the material. First, a review of the parameters of LPF processing, the forming mechanisms, process modeling techniques, and alternative LPF methods is discussed, to understand the procedures of industrial manufacturing standards. Next, a simplification of metallic thin foils is proposed to develop a novel low-cost and simplified LPF process design.

The first segment pursues the general principles of LPF by reviewing its recent progress, and that of comparable techniques. It discusses the process design, mechanisms attributed to forming, laser-material interactions, simulation methods, alternative approaches, and limitations thereof. The effect of laser intensity, material thickness, overlapping ratio, and number of scan tracks on bend angle, is discussed. Mechanisms of LPF are reviewed by elucidating the mechanics of convex and concave curvature. Particularly, the Stress Gradient Mechanism (SGM) and the Stress Bending Mechanism (SBM), are modeled. In addition, the effect that drag bending has on the net bending of the sample piece is considered. The Fabbro model is followed for laser-material interactions. Advances in femtosecond and heat assisted LPF are considered with a focus on the advantages and disadvantages over nanosecond methods.

In the second segment, a streamlined LPF process design that eliminates ablative coating and confining media is developed and explored to determine the feasibility of

bending of thin metallic foils. Experiments were conducted in a fashion similar to traditional LPF processing, with additional equipment unique to this new method, to determine the final bend angle. Evidence has shown that laser intensity, sample thickness, and material strength are primary parameters in determining bending direction, amplitude and process efficiency. In this part of the study, the effect of the number of passes and laser intensity on bending angle was examined. The results show that with increasing number of passes, there is an increase in bending angle, and, likewise, with an increase in laser intensity, there is an increase in bending angle. Then, the surface profile of the sample was inspected, and the laser-processed area was characterized with respect to surface roughness. It was found that, relative to the original sample, the surface roughness of the laser-processed area was not significantly impacted. Finally, the bend angle of LPF with and without an ablative coating, using equivalent experimental parameters, was compared. This portion of the study indicates that using an ablative coating under this new LPF process design is counterproductive.

ACKNOWLEDGEMENTS

I would like to thank my advisor, Dr. Yiliang Liao, for his continued encouragement and support in research opportunities at the University of Nevada, Reno. His guidance and expertise have directed me throughout the entire process of research and writing of this thesis. He is an inspiration to my dreams for a higher education. I would also like to thank Dr. Matteo Aureli, and Dr. Bin Li, who have been magnificent mentors, and have motivated the pursuit of my studies. They are the finest examples of academic leaders.

Additionally, I would like to thank Cindy Veschi for her steadfast support, being not only a great mentor, but a wonderful friend. Her selfless care and loving attitude sets an example to everyone she meets and inspires me to pay if forward. Also, I would like to thank Terry Heckler for his enduring friendship and guidance throughout my educational experience. He is the illustration of gentleman.

Finally, I would like to thank my family – father, mother, and two sisters – for their love and encouragement during the last few years of my educational career.

TABLE OF CONTENTS

LIST OF TABLES……...……v

LIST OF FIGURES…..……..…vi

CHAPTER 1

1. INTRODUCTION 1
2. LASER PEEN FORMING 3
   - 2.1 Process Design 3
   - 2.2 Processing Parameters 4
     - 2.2.1 Laser Intensity 5
     - 2.2.2 Material Thickness 6
     - 2.2.3 Overlapping Ratio 7
     - 2.2.4 Number of Scan Tracks 8
   - 2.3 Transitional Thickness 9
3. FORMING MECHANISMS 10
   - 3.1 Physical Principles of LPF 10
   - 3.2 Bending Modes of LPF 10
     - 3.2.1 Convex Bending 13
     - 3.2.2 Concave Bending 15
     - 3.2.3 Drag Bending 17
4. PROCESS MODELING 20
   - 4.1 Laser-Material Interaction - Fabbro's Model 20
   - 4.2 Finite Element Analysis 22
     - 4.2.1 Simulation and Numerical Analysis of LPF 22
     - 4.2.2 Simulation Results 25
5. ALTERNATIVE METHODS 28
   - 5.1 Femtosecond Laser Peen Forming 28
   - 5.2 Heat Assisted Nano-Second Laser Peen Forming 29
6. CONCLUSION 32

CHAPTER II

7. LASER PEEN FORMING WITHOUT ABLATIVE COATING AND CONFINING MEDIA 33

7.1 Background and Motivation 33
7.2 Experiment.....33
7.2.1 LPF without ablative coating and confinement 33
7.2.2 Characterization and Measurement.....36
7.3 Experimental Results and Discussion.....38
8. CONCLUSION 42
REFERENCES.....43

LIST OF TABLES

Table

1. Laser parameters for LPF without ablative coating and confining media……..... 35
2. Experiment details for study on effect of number of passes on bend angle ….....35
3. Experiment details for study on effect of laser intensity on bend angle ……36

LIST OF FIGURES

Figure

1. Schematic of LPF experimental setup with (a) Diagram of LPF system showing mounted sample assembly, platform, and laser path, and (b) The sample assembly with representative laser-induced shockwave ……..3
2. Development of irradiated pulses producing scanning pattern.....4
3. Effect of laser intensity on bend direction and magnitude 6
4. Bending angles for various thickness sheet metal using 0.2 J, 0.3 J, 0.4 J, 0.5 J laser energies 7
5. Effect of overlapping ratio, OR, on bend angle for different thickness samples.....8
6. Effect of number of scan tracks on bending behaviors of 1060 commercial pure aluminum sheets with thickness of: (a) 0.5 mm, and (b) 2 mm.....8
7. Principle of laser peen forming during (a) Irradiation and (b) Deformation stages.....11
8. Transition from convex to concave bending.....12
9. Development of the SGM in LPF convex Bending: (a) Surface shock loading; (b) Stress gradient formation; (c) Stress gradient relaxation producing bending; (d) Cellular moment produced after irradiation; (e) Global bending of specimen.....14
10. Development of the SBM in LPF concave bending: (a) Surface shock loading; (b) Downward plastic deformation; (c) Bending; (d) Cellular moment produced after irradiation; (e) Global bending of specimen.....16
11. Schematic diagram of types of bending in thin sheet deformation.....18
12. Effect of drag bend on net bending angle 19
13. Target assembly geometry during confined ablation process.....20
14. FEM logic flow chart.....24
15. FEA Simulation Configuration.....25
16. Simulation results of bending deformations for different thickness of sheet metal 26
17. Simulated deformation of different pulse energies.....27
18. Laser-assisted local heating LPF 29
19. Effect of laser assisted local heating LPF on (a) Arc height and (b) Curvature radius 30

20. Schematic of LPF experimental setup without ablative coating and confinement....34
21. Schematic of (a) Bending detection equipment and (b) Geometry model used to calculate bending for angles less than 10°....36
22. Samples of AA 1100 at 20x magnification for (a) pre-processing, and (b) post-processing, and 50x magnification for (c) pre-processing, and (d) post-processing....38
23. Effect of number of passes on bending angle of AA 1100 for laser intensities of (a) 0.6 GW/cm2 and (b) 3.6 GW/cm2....39
24. Effect laser intensity on bending angle of (a) AA 1100 (b) SS 304 and (c) AA 6061-T6....40
25. Comparison of 0.254 mm thick AA 1100 with and without ablative coating....41

CHAPTER I

1. Introduction

Laser Peen Forming (LPF), an application of Laser Shock Peening (LSP), is a non-contact sheet metal forming process using high pressure, compressive shock waves induced by a pulsed laser system to modify curvature via beneficial residual stresses. In 2002, Hackel and Harris [1] developed a system using this exact method to form strips of sheet metal. LPF couples the benefits of inducing residual stresses during LSP processing with tool free bending to shape metallic parts as small as the micro-scale, with high accuracy. It allows sheet metal to be bent, shaped, and precision-aligned with the use of straight or curved laser scan lines to acquire desirable three-dimensional (3D) features on micro-components with bending angles less than 10° [2]. LPF is of significant value to industries such as aerospace (aircraft skin panels [3]), automotive, shipbuilding, microelectronics and microelectromechanical systems [4, 5] that previously relied on expensive stamping dies, because it avoids imparting detrimental stresses to the material.

Unique characteristics of LPF include its non-thermal approach [6] and ability to bend material in either the positive (toward beam) or negative (away from beam) directions without changing the setup. Traditional methods of laser forming rely on introducing thermal stresses to the work piece via irradiation. For this type of processing, the cooler (ambient) material restrains the thermal expansion of the heated area at the laser-material interaction site, leading to deformations. The thermal expansion and shrinkage impart stresses to the component, which are balanced by distortions and stress redistributions, resulting in bending [5]. Conversely, LPF's non-thermal bending mechanisms protect the

target material from unwanted thermally induced stresses and make it possible to form without material degradation. Pence, C., et al [2, 4] explained that, during the LPF process, short laser pulse irradiation duration is required, which is in the range of nanoseconds and several-orders less than the radiation time required to initiate the thermal forming mechanism.

In addition, it offers improved mechanical properties, fatigue performance, and microstructural stability in the processed part by means of compressive residual stresses. Hu et al [7] categorized and described the bending mechanisms during LPF processing of sheet metals by introducing the SGM and SBM. LPF also has many technological advantages including design flexibility to produce complex shapes. In the interest of investigating primary processing parameters, Sagisaka, et al [3] performed experiments with pure aluminum, phosphor bronze and stainless steel to relate the deformation modes (positive or negative bending) to the peening energy, work piece thickness, and hardness. LPF surpasses traditional forming methods by providing a spring back free, non-contact forming technique that requires no hard tooling or external forces. It has the potential to process materials which are either extremely difficult or impossible to bend mechanically.

2. Laser Peen Forming

2.1 Process Design

Fig. 1(a) illustrates a typical optical system arrangement, mounting provisions for the sample assembly, containment of the confining media, and sample position control via X-Y stages. A Q-Switched Nd:YAG nanosecond pulsed laser system operating at 1,064 nm wavelengths provides the necessary laser requirements for an LPF experiment. Fig. 1(b) details the sample assembly: An ablative coating is applied to the top surface of the sample to absorb incident laser energy and protect the surface from unsolicited damage.

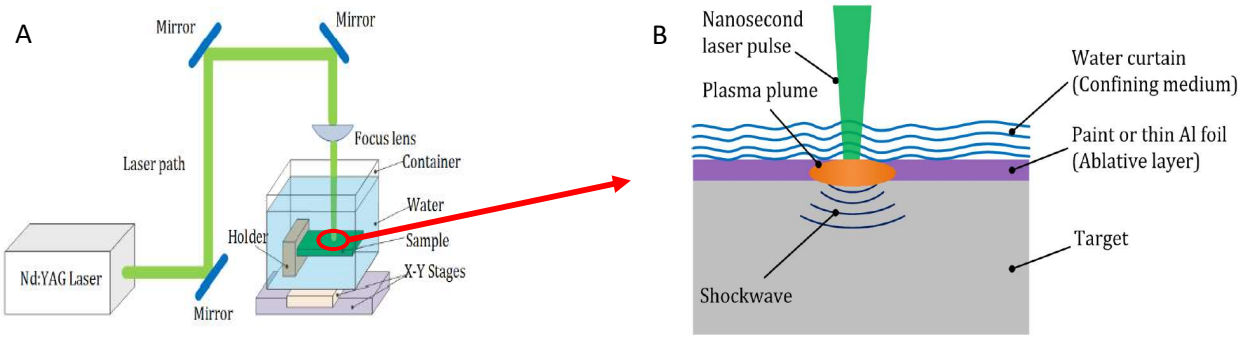

Fig. 1 – Schematic of LPF experimental setup with (a) Diagram of LPF system showing mounted sample assembly, platform, and laser path, and (b) The sample assembly with representative laser-induced shockwave. Adopted with permission from [2, 4]

The cantilevered sample assembly is submerged under water within a container which rests atop two stages. Each stage is oriented 90° relative to one another, providing planar motion of the sample, normal to the direction of the incident beam. The laser beam is directed to the target through a series of reflecting mirrors and a convergent lens. When a high-intensity pulse is injected to the sample surface, the ablative coating is instantaneously

vaporized, then ionized [3, 8, 9], forming a high pressure, rapidly expanding plasma. As a result, a shockwave is induced due to the ultrafast expansion of plasma. A confining medium is employed to resist the hydrodynamic expansion of the plasma and enhance the shock pressure, providing higher residual stresses via plastic deformation. Materials such as black tape, aluminum and graphite can be used as ablative coatings, while water is most commonly chosen to be the transparent confining media.

2.2 Processing Parameters

Fig. 2 shows the laser scanning path and parameter settings during the experiment. Scanning begins on one side of the work piece, at a distance, d, from the fixed end. Once the laser pulses have traversed the sample width, a step interval, Δx, along the length

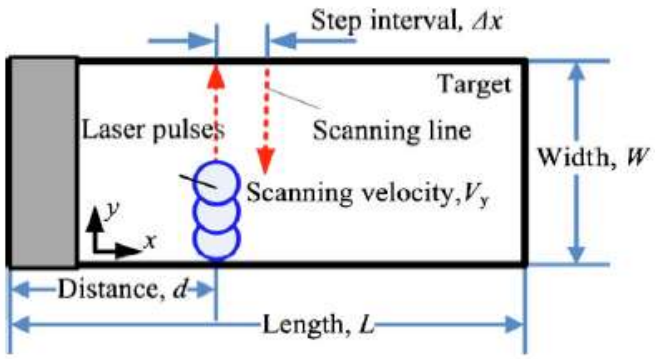

Fig. 2 – Development of irradiated pulses producing scanning pattern, adopted with permission from [12]

direction, L, occurs. When the step interval is complete, the sample returns in the opposite direction along the width of the sample, producing another scan line. This repeats until the total number of prescribed scan lines, n, has been achieved. The process starts again from the beginning and repeats until the desired number of passes, p, has been attained. For LPF,

the sample material thickness, and laser power intensity are the most critical parameters for predicting the bending mode, which describes bending direction. For a certain material with a fixed thickness, as laser intensity increases, bending direction changes from convex (away from beam) to concave (toward beam) due to the residual stress distribution throughout the thickness generated by the laser-induced shockwave. For a fixed laser intensity, the shockwave penetration depth is constant. In this case, decreasing the material thickness will modify the ratio of the compressive residual stress penetration depth to specimen thickness, ultimately leading to a transition from convex to concave bending. Additional laser parameters such as overlapping ratio (or laser scan speed) and number of scan tracks affect the magnitude of the bend exclusively, and should be adjusted for process optimization.

2.2.1 Laser Intensity

For a specific material with a given thickness, the parameter governing the magnitude and direction of the bend is laser intensity. Ding, et al [4] demonstrated this concept using laser intensities of 0.2 J, 0.3 J, 0.4 J and 0.5 J on Aluminum Alloy 1060 samples with thicknesses of 0.70 mm, 0.88 mm, 1.07 mm and 1.75 mm. Fig 3 illustrates that both concave and convex curvature was attained for each laser intensity. It can be deduced that the transitional thickness threshold from concave to convex bending at 0.2 J and 0.3 J is approximately 0.88 mm, and increases with an increase in laser intensity, as indicated by the increasing concave bending of the 0.88 mm sample at 0.4 J and 0.5 J.

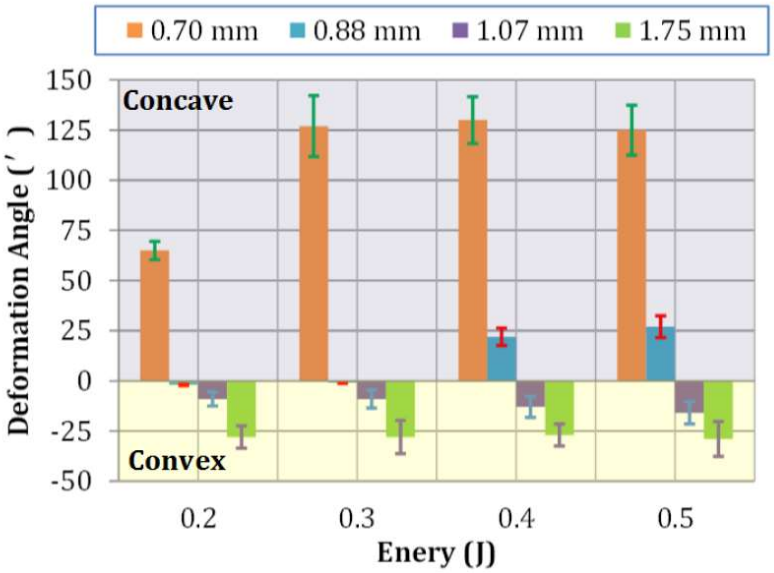

Fig. 3 – Effect of laser intensity on bend direction and magnitude, adopted with permission from [4]

2.2.2 Material Thickness

Several research experiments have been conducted that investigate how the thickness of a sample affects the final bending angle. Pence [4] studied the effect of sample thickness on the bend angle of Aluminum 1060 using four distinct laser intensities. By setting constant the number of scan lines, n = 5, and Overlapping Ratio, OR = 63%, the thickness threshold zone for Aluminum 1060 was determined. The laser intensities corresponding to 0.2, 0.3, 0.4, and 0.5 J are 1.2, 1.8, 2.4, and 3.0 GW/cm^2, respectively. It was revealed that a critical thickness threshold exists between 0.7 and 0.88 mm where the sample transitions from positive to negative bending. A summary of the results for applying four separate laser intensities on material thicknesses of 0.70, 0.88, 1.07, and 1.75 mm is shown in Fig. 4. In addition, a finite element solution validated that thoroughly strained specimens produce concave bending and that as the ratio of plastic deformation penetration to specimen thickness, A, decreases to substantially less than unity, the negative bending

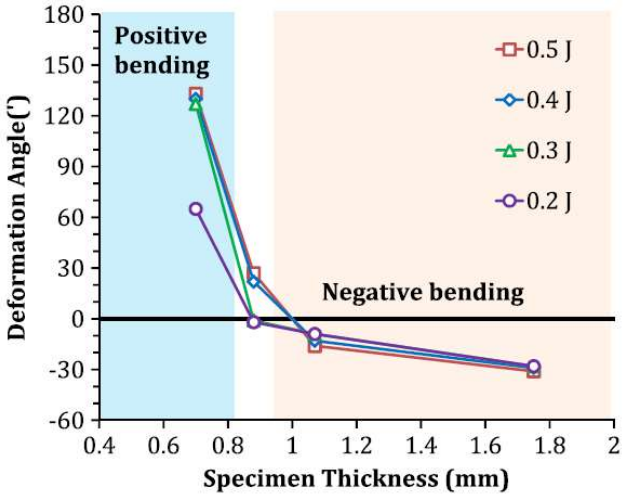

Fig. 4 – Bending angles for various thickness sheet metal using 0.2 J, 0.3 J, 0.4 J, 0.5 J laser energies, adopted with permission from [2]

mechanism takes over, and the sample experiences convex bending. The ability to predict the final bend angle, considering all forming mechanisms, has prompted a plurality of investigations into simulating the LPF process.

2.2.3 Overlapping Ratio

By changing the scanning velocity, the Overlapping Ratio, OR, can be adjusted. The OR is the ratio of the distance a subsequent beam spot overlaps a previous beam spot to the spot size, in the direction of the scanning path, as a percentage. Two beam spots tangent to one another represent an OR of 0%, and two beam spots concentric to each other represent an OR of 100%. Typically, this information is presented as experimental parameters spot size (beam diameter), laser repetition frequency, and scanning velocity. For a given spot size and laser frequency, an increase in scanning velocity leads to a decrease in OR, and a decrease in bending angle. Fig. 5 demonstrates the effect a change in OR has on three different thickness sample pieces.

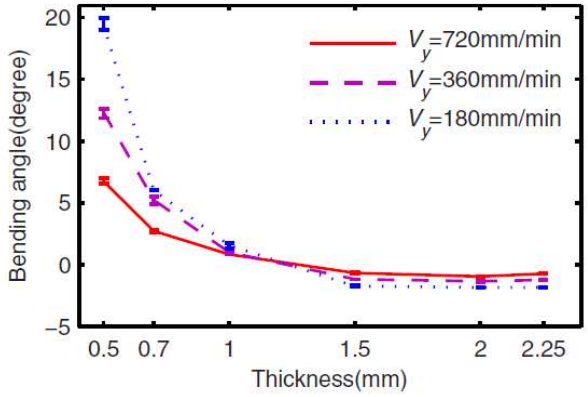

Fig. 5 – Effect of overlapping ratio, OR, on bend angle for different thickness samples, adopted with permission from [7]

2.2.4 Number of Scan Tracks

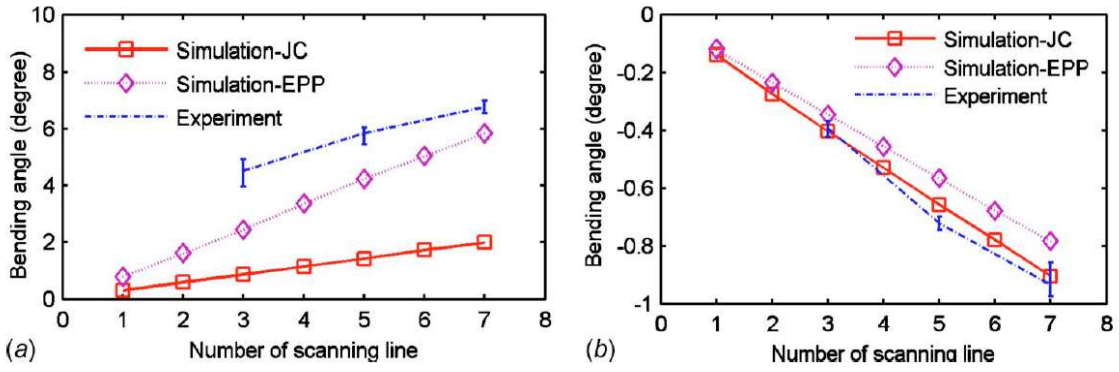

Fig. 6 - Effect of number of scan tracks on bending behaviors of 1060 commercial pure aluminum sheets with thickness of: (a) 0.5 mm, and (b) 2 mm. Adopted with permission from [12]

The number of scanning tracks plays another critical role on determining the bending behaviors of work pieces subjected to LPF. Fig. 6 (a) and (b) show the experimental and finite element simulation results of LPF of 1060 commercial pure aluminum sheets with thickness of 0.5 mm and 2 mm, respectively. It is found that the bending angle is accumulated by increasing the number of scanning tracks. For the sample

with a thinness of 0.5 mm, given a laser intensity of 3.85 GW/cm2, a laser spot radius of 0.6 mm, and a laser scanning velocity of 720 mm/min, the concave bending angle is increased from around 4 to 6.77 degree by increasing the scanning number from 3 to 7. On the other hand, given the same laser processing parameters, for the sample with a thickness of 2 mm, the convex bending angle increases by 0.8 degrees from -0.16 to -0.96 degrees with the increase of scanning number from 1 to 7. As shown in Fig. 6, both experimental and simulation results indicate that the number of scanning tracks determines the accumulated bending angle, while not affecting the bending curvature direction (concave or convex), which is mainly determined by the sample thickness and laser intensity.

2.3 Transitional Thickness

Every material has a critical thickness threshold that transitions the bend direction from concave to convex bending. The ratio of the compressive residual stress penetration depth to specimen thickness is critical in determining this bending mode, and is denoted as A [4]. For a given laser intensity, beginning with a material thin enough to initially produce concave bending, increasing the material thickness, decreases A. By continuing to increase the sample thickness, convex bending ultimately realized. Increasing laser intensity along with material thickness gives rise to an increase in transitional thickness through an increase in the ratio of residual stress penetration to material thickness, A. It is therefore important to investigate how the sample responds to changes in laser intensity and material thickness.

3. Forming Mechanisms

3.1 Physical Principles of LPF

LPF, a derived application of LSP technology, is a method of purely mechanically forming a target to modify its curvature through the introduction of laser energy to the sample material. When a high energy, short pulse, focused laser beam is directed on to the surface of sheet metal, the surface instantaneously ionizes, and is vaporized. This generates a rapidly expanding, high pressure plasma, produced locally about the laser beams travel axis, normal to the surface of the sheet metal. Introducing a confining media, such as water, traps the expanding plasma, and re-directs it toward the sheet metal, where it violently explodes against its surface. By magnifying the pressure against the surface of the sheet metal with the confinement media, a transient rise in pressure forms a shockwave, reaching values exceeding 1 GPa.

The relationship between the shockwave pressure and the plastic deformation has been investigated extensively. During the scanning of the laser pulse on the surface of the sample, plastic deformations will occur if the laser-induced shockwave peak pressure is greater than the Hugoniot elastic limit (HEL) of the sample, as shown in Fig. 7 (a). No plastic deformation or residual stress are observed when the shockwave pressure is less than the HEL. Typically, plastic deformation increases linearly with the shockwave pressure within 1 HEL and 2 HEL range, which is the usual working condition for LPF [4].

Under such a circumstance, the mechanisms of concave and convex bending have been investigated and is attributed to the ratio of compressive residual stress penetration depth and the thickness of the sample material, A. Once the shockwave pressure exceeds the

HEL, plastic deformations will occur underneath the laser-scanned area. Hence, the material forms via compressive residual stress within this region, as shown in Fig. 7 (b). The penetration depth of such a compressive residual stress is determined by the energy of the laser pulse and the properties of the target material. In general, the higher the intensity of the laser pulse, the deeper the compressive residual stress will reach.

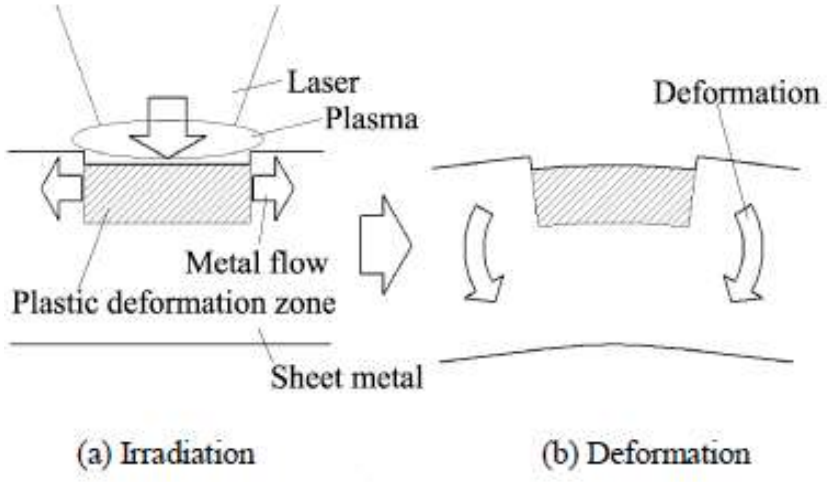

Fig. 7 – Principle of laser peen forming during (a) Irradiation and (b) Deformation stages, adopted with permission from [3]

3.2 Bending Modes of LPF

The bend is classified by bend direction, which is determined by the depth of the plastic deformation zone [10]. Fig. 8 demonstrates how adjusting the parameters affecting the bending mechanism could affect the bending mode. Mode I & II correlates to negative, or convex, bending. Mode I occurs when the plastic deformation depth is shallow enough, such that only the peened surface is deformed. When the deformation depth is deep enough to reach the bottom surface, Mode II is enabled, and the residual stresses induced on the

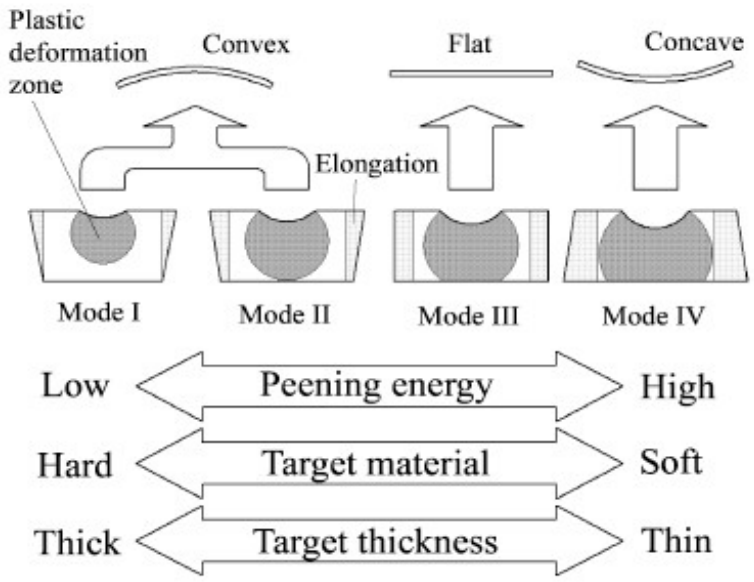

Fig. 8 – Transition from convex to concave bending, adopted with permission from [3]

bottom surface begin to counteract the effects of the plastic deformation zone on the top surface. When the growth of the deformation zone on the bottom surface reaches that of the top surface, Mode III is realized, and the work piece is kept flat. As the deformation zone on the bottom surface continues to develop such that it exceeds the deformation zone of the top surface, Mode IV is achieved, and the curvature of the peened surface is positive, or concave.

It is essential to determine and control the penetration depth of the shockwave pressure to predict the bending direction. The penetration of the shockwave, and subsequently, the depth of plastic deformation into the thickness of the material ultimately determines the bend direction of the sample. For a fixed laser intensity, the dominant factor in positive-negative bending is the thickness of the material. The LPF process can be separated in to three steps, (1) generating the shockwave; (2) imparting residual compressive stresses in

to the thickness of the sample via the shockwave; and (3) relaxation of compressive residual stresses to produce bending. During the LPF process, as the shockwave propagates in to the material, plastic deformation occurs to a depth where the leading shockwave pressure remains greater than the dynamic yield strength of the material. The point at which the shockwave pressure ceases to induce plastic deformation is known as the Hugoniot Elastic Limit (HEL). According to Johnson and Rohde [11] the HEL of the target metal relates to the dynamic yield strength as follows: $HEL = \frac{1-\nu}{1-2\nu}\sigma_y^{dyn}$, where ν is Poisson's ratio and σ_y^{dyn} is the dynamic yield strength at high strain rates. As the shock wave pressure increases to above 1 HEL, plastic deformation and strain increase, reaching further into the sample material. By increasing laser intensity, and therefore, shockwave pressure, four distinct modes of bending can be achieved. To distinguish between positive (convex) bending and negative (concave) bending, Hu, et al proposed the stress gradient mechanism (SGM) and the shock bending mechanism (SBM) [7]. To account for the bending moment effect at the clamped end produced by the application of the laser pulse, Ocaña, et al 26] developed the drag bending concept.

3.2.1 Convex Bending

With relatively low laser intensity and thick sample material, such as 1.8 GW/cm^2 applied to 1.75 mm Aluminum 1060, negative bending, can be achieved [2]. The SGM model, shown in Fig. 9, is used to describe how this convex curvature is attained. After the laser-induced shockwave is initiated into the surface of the material, it attenuates quickly, as shown in Fig. 9 (a). However, for pressures large enough to generate plastic deformation, the material thickness within the shock region is compressed, as portrayed in Fig. 9 (b).

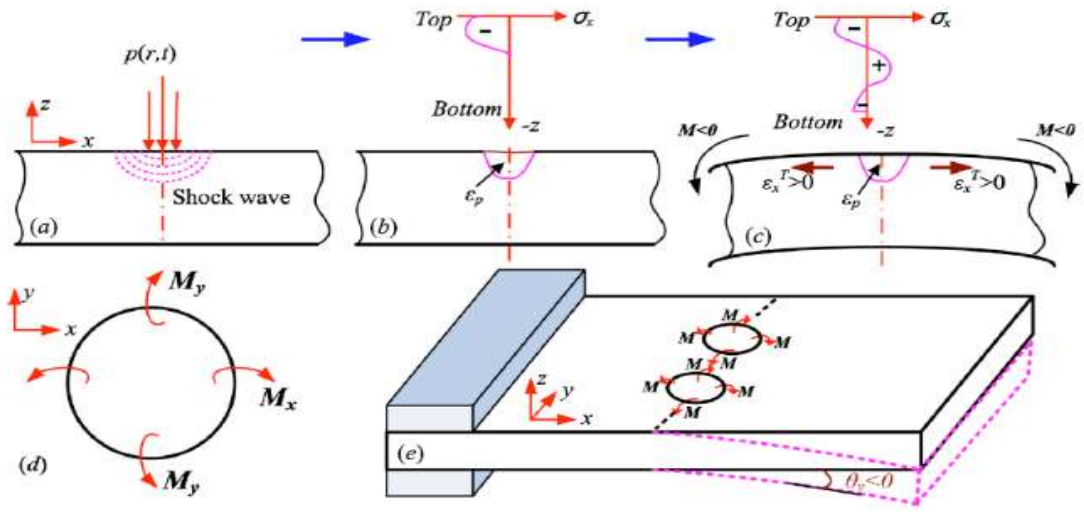

Fig. 9 – Development of the SGM in LPF convex Bending: (a) Surface shock loading; (b) Stress gradient formation; (c) Stress gradient relaxation producing bending; (d) Cellular moment produced after irradiation; (e) Global bending of specimen, adopted with permission from [7]

Subsequently, the material beneath the top surface of the shocked region experiences tension along the horizontal direction. Continuing toward the bottom surface of the sample piece, the displacement of the material due to tensile stress is restricted by the surrounding material, generating compressive stresses within the laser-shocked region. Once effective stresses reach strain rate dependent flow stress, additional material flow translates into plastic strain which decreases monotonically with respect to the thickness of the material below the top surface [7].

If the sample is thick, or the laser intensity is low, plastic deformation is restricted to just beneath the top surface, only slightly penetrating the top surface of the sample. When the shock wave ceases to effectuate plastic deformation, a precipitous compressive stress gradient develops, decreasing monotonically, as shown in Fig. 9 (b). During this tensile stress relaxation period, the compressive stress gradient is partially relaxed to satisfy the geometric compatibility shown in Fig. 9 (c). This produces a moment according to Fig. 9

(d), and tensile strain at the top layer of the sample, expanding laterally toward the free end of the specimen, as shown in Fig. 9 (e). Thus, the sample bends away from the laser beam, producing a convex curvature. Once steady state has been reached, both top and bottom surfaces may be in a state of compression, leaving the shocked areas in an advantageous state for fatigue and corrosion resistance [12]. For isotropic materials clamped on one end, as in LPF, bending occurs along the scanned line and consists of an accumulation of superimposed shock regions. Thus, downward bending of the free end is generated by the SGM.

The amount of bending for convex curvature mostly depends on the compressive stress gradient. An increase in material thickness requires an increased moment to produce the same bending angle. Therefore, with constant laser intensity and increasing material thickness, a smaller bend angle is obtained. Eventually, when the thickness is large enough, a saturation point is reached, and only a compressive stress field is left on the top surface without any bending. Increasing the number of laser shocks used in LPF processing contributes to an increase in bend angle.

3.2.2 Concave Bending

By changing one or more of the critical processing parameters, a transition to the SBM allows for a positive, toward-beam bending mode. This concave bending curvature is depicted in Fig. 10. The strength of the shockwave decays quickly during the propagation into the work piece, where plastic deformation occurs for as long as the shockwave strength is greater than HEL. In this case, for a sufficiently thick sample, the penetration depth is a fixed value for shockwave affected region. For a very thin sample, the strength of

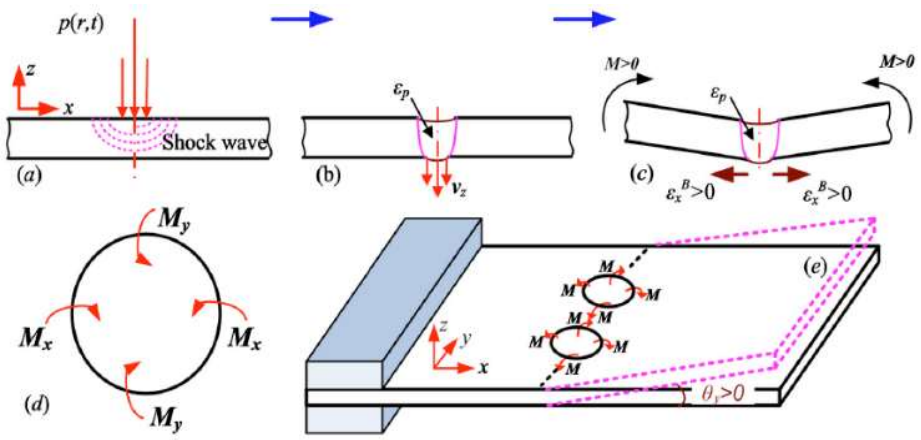

Fig. 10 – Development of the SBM in LPF concave bending: (a) Surface shock loading; (b) Downward plastic deformation; (c) Bending; (d) Cellular moment produced after irradiation; (e) Global bending of specimen, adopted with permission from [7]

shockwave does not fall below the HEL limit before reaching the bottom surface. As a result, the shockwave can penetrate the full sample, leaving the entire thickness of the material experiencing plastic deformations, as represented graphically in Fig 10 (a). Downward loading from the shockwave transmits inertia to the sample within the shock region, downwardly, as shown in Fig. 10 (b). This continues during the relaxation period, and the shock region experiences plastic deformation. Different from the convex bending mechanism, the concave bending mode is achieved by the downward inertia through the full cross-section. Due to this extreme shock loading, the sample is completely plastically deformed throughout its thickness, and a very small stress gradient subsists between the top and bottom surface of the material, compared to convex bending mode values. The downward plastic deformation generates a positive moment within the shock region, as shown in Fig. 10 (c). A view of the local cell indicating the location of the moment is shown in Fig. 10 (d). The tensile material flow at the bottom surface, within the shock region, expands toward the free end of the cantilevered sample, generating the convex

curvature acquired in the LPF process, as shown in Fig. 10 (e). Like convex bending, concave bending occurs along the scanned line and consists of an accumulation of superimposed shock regions.

Since bend direction primarily depends on the amount of plastic deformation through the thickness of the material within the shock region, if material thickness increases, a larger cellular moment is required to produce a similar bending angle. The moment produced on the bottom surface is reduced and the positive curvature of the sample is decreased. Therefore, for a fixed laser intensity, increasing material thickness decreases the concave bend angle in the SBM. Correspondingly, for a fixed material thickness, an increase in laser intensity leads to a higher shock pressure and therefore promotes the depth of plastic deformation into the cross-section, producing an increase in bend angle. Outside the local shock region, additional forming mechanisms may be occurring. The bending moment placed on the sheet metal by drag bending could add to the overall bend angle, and curvature, of the sample.

3.2.3 Drag Bending

The laser ablation process requires a very high pulsed laser intensity, normally exceeding 1 GW/cm^2 [13]. Accordingly, pressures above 1 GPa stress the material, dynamically deforming it with strain rates beyond 10^6 s^{-1} [6, 13]. The application of this large pressure at a distance, d, from the mounting location, can generate a bending moment that affects the net bend angle of the sample. If the bending moment is great enough to plastically deform the material according to beam theory, a drag bend is generated, causing the sample material to bend away from the laser beam. The residual stress gradient

produced by the bending moment is opposite the shockwave induced residual stress gradient of SGM and SBM, with tensile stresses present on the top surface and compressive stresses on the bottom surface, as seen in Fig. 11. Therefore, in the case of concave bending,

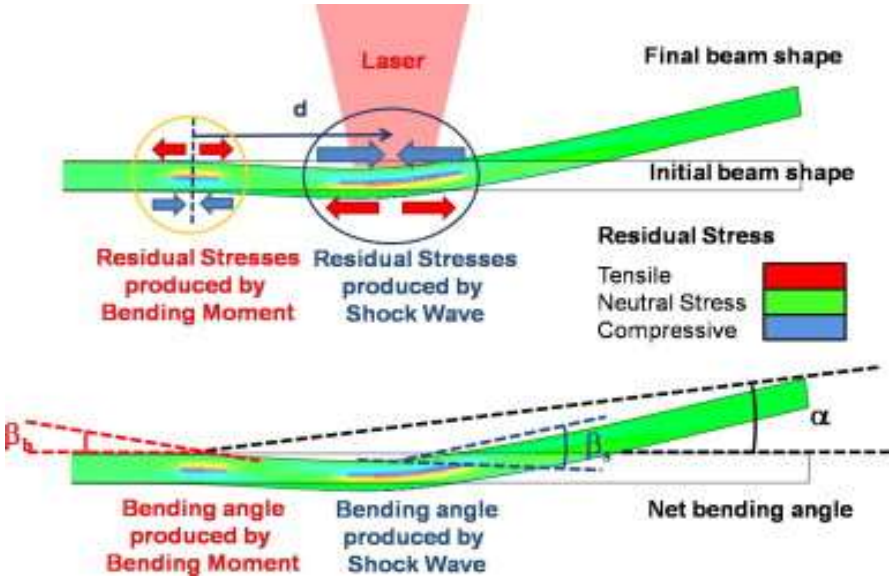

Fig. 11 – Schematic diagram of types of bending in thin sheet deformation, adopted with permission from [26]

SBM residual stresses produced by the shockwave add to the positive curvature of the sample. Contrarily, residual stresses produced by the drag bend moment subtract from the overall curvature of the sample. The net bending angle is the superposition of these bend angles, as indicated by Fig. 12. Like SGM and SBM, total drag bending angle is produced by the accumulation of drag bend angles produced by each laser pulse.

Processing parameters affecting the drag bend include laser intensity, distance from clamping end, ablative material properties and thickness, sample material properties and thickness, and confinement media type and height above the sample surface. J.L. Ocaña,

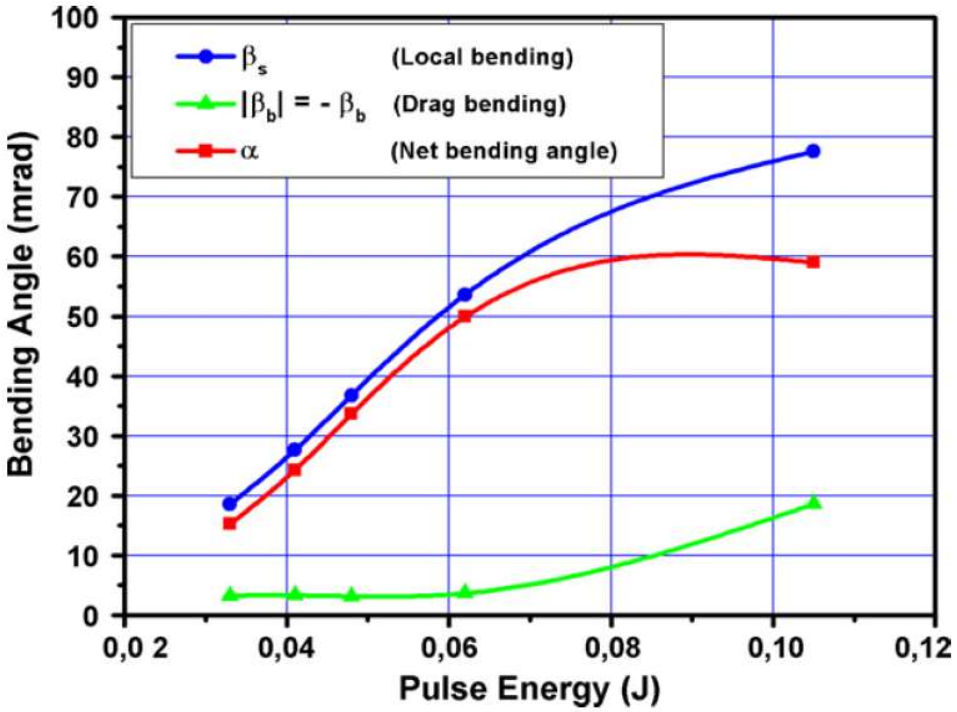

Fig. 12 – Effect of drag bend on net bending angle, adopted with permission from [26]

et al [26] demonstrated that after a critical value of laser intensity, the drag bend generated by the bending moment begins to have a greater impact on the net bend angle. As the pressure increases at the laser induction site, the residual stress distribution reaches a saturation limit. The shockwave pressure therefore has an increasing effect on the bending moment, which translates to a larger drag bend.

4. Process Modeling

4.1 Laser-Material Interaction - Fabbro's Model

The most extensively used model is developed by Fabbro, et al [14-16]. This model is based on work pioneered by O'Keefe, et al [17], Yang, et al [18] and Anderholm, et al [19-21]. Fabbro's model investigates the laser material-interaction under confinement, in three steps: (1) during the laser material interaction, pressure is generated by the shockwave that is induced by plasma expansion under the confinement media, (2) after each pulse terminates, the expanding plasma gas maintains this pressure and then decays due to an adiabatic cooling process, and (3) at a sufficiently long time, the plasma expansion accumulates, introducing additional momentum to the target.

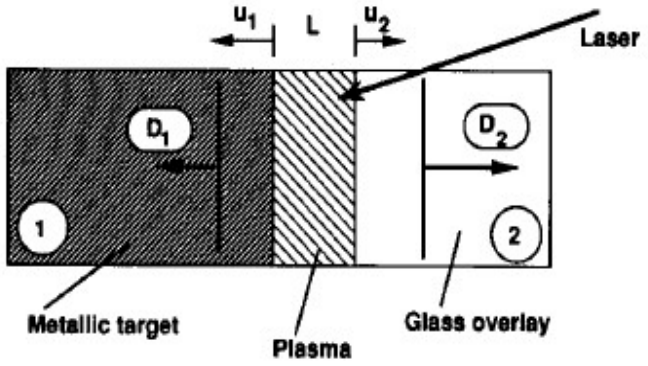

Fig. 13 – Target assembly geometry during confined ablation process, adopted with permission from [14]

As shown in Fig. 13, after the pulse is injected on the interface of the confinement and ablative coating, the coating layer is immediately heated, vaporized and ionized into plasma. The plasma gas expands ultrafast into the adjacent layers, generating a shockwave that propagates into neighbor mediums. Therefore, Fabbro, et el [14-16] assumes the

displacement of the interface wall is caused solely by plasma expansion behind the shockwaves.

The increasing thickness of the plasma layer, as a function of time, is denoted by $L(t) = \int (u_1 + u_2)\, dt$, where u_1 and u_2 are plasma expansion velocities towards the substrate and confinement. Two scenarios for the confinement medium are considered: (a) solid confinement and (b) gas confinement. For (a), the plasma expansion speed is written as $\frac{dL(t)}{dt} = \frac{2}{Z} P(t)$, where $\frac{2}{Z} = \frac{1}{Z_1} + \frac{1}{Z_2}$, and the pressure is given by $P = \rho_i D_i u_i = Z_i u_i$, where ρ_i, D_i, Z_i are density, shock velocity and shock impedance of material *i*. In the case of gas confinement (b), the relation is given by $P(t) = K(\frac{dL}{dt})^2$, where $K = \frac{(\gamma+1)\rho_0}{8}$, $\frac{2}{\sqrt{\rho_0}} = \frac{1}{\sqrt{\rho_1}} + \frac{1}{\sqrt{\rho_2}}$ and γ is the Gruneisen constant. Once the plasma is formed, the laser pulse energy is absorbed by the plasma plume, and its internal energy increases, promoting its expansion. The energy conservation equation is described as

$$I(t) = P(t)\frac{dL}{dt} + \frac{d}{dt}(E(t)L) \tag{1}$$

Where $E(t)$ represents the total internal energy, $I(t)$ represents the laser intensity, and α is a constant representing the thermal energy component of the total internal energy, with the remaining total internal energy, $1 - \alpha$, being used for ionization. Under an ideal gas assumption, the equation of state is written as $P = \frac{2}{3}\alpha E(t)$. Finally, Eq. 1 is written as

$$I(t) = P(t)\frac{dL}{dt} + \frac{3}{2\alpha}\frac{d}{dt}(P(t)L) \tag{2}$$

For the general case, the above equations can be integrated numerically to obtain the pressure evolution as a function of time. Under the simplest assumption - that the laser

intensity is a constant and initial condition $L(0) = 0$ - Fabbro's model can provide an analytical result for pressure and the thickness of the plasma layer.

$$\text{Case (a)} \qquad P = 0.1\sqrt{\frac{\alpha Z I_0}{2\alpha+3}}\ , \qquad L(t) = 2 \times 10^4 P\ t\ Z^{-1} \tag{3}$$

$$\text{Case (b)} \qquad P = 32.2\left(\frac{\alpha I_0}{2\alpha+3}\right)^{2/3} \rho_0^{1/3}\ , \qquad L(t) = 0.55\ t\ \sqrt{P/\rho_0} \tag{4}$$

where P is in the unit of kbars, I_0 is in the unit of GW/cm^2, t is in the unit of nano-second, ρ_0 is in the unit of g/cm^3 and L is in the unit of micro-meter.

4.2 Finite Element Analysis

4.2.1 Simulation and Numerical Analysis of LPF

The simulation and analysis for the transition of the concave and convex bending are studied by Ding, et al [4]. For thin aluminum sheet metal under single-sided laser peening configuration, they found the transition mechanism of the concave-convex bending during the LPF process was related on the energy of laser pulse and the thickness of aluminum sheet metal. Once an ultra-short laser pulse is injected into the metal surface, the energy of the incident photons is instantaneously absorbed by the free electrons at the metal surface since the heat capacity of the electrons is much lower than that of lattices. Within the femtosecond regime, the absorbed energy is re-distributed among the free electrons by electron-electron collisions and finally thermalized into the electron gas, leaving the host lattice temperature temporarily unaffected. Subsequently, in the picosecond time scale, the highly non-equilibrium electrons with extremely high temperature start to transfer thermalized energy to the lattice via electron-phonon collisions. The energy exchange between electrons and lattice typically last a few tens of picoseconds before finally

reaching thermal equilibrium. As a result, the surface of the metal is vaporized. The vaporized particles keep absorbing energies from the laser pulse and finally they are ionized into plasma. Plasma gas absorbs energy from laser pulse and expands rapidly. The ultrafast expansion of such a laser-induced plasma is trapped by the confining media and redirected towards the target material, introducing a shocking pressure wave that propagates into the target material. With the aid of confinement, the magnitude of this shock pressure is typically on the scale of a few GPa. Plastic deformation occurs once the peak pressure of the laser-induced shockwave exceeds the dynamic yield strength of the material. Coincidentally, the shockwave penetrating the sheet metal generates a compressive plastic deformation layer around 1mm in depth. As a result, the sheet metal will deform either concave or convex to balance such a residual stress at the yield region. However, the actual transient response during the LPF process is extremely complicated, since very high stress loadings are applied on the surface of the sample during a very short pulse duration. Therefore, a numerical analysis is introduced to simulate and understand the response during the transient state in LPF. Due to the nature of complications in the transient state, the conventional explicit FEA algorithm is not applied here since the convergence efficiency toward the stable residual stress field is extremely low. Instead, Ding et al develop a multi-level FE model. The approach obtains the results from an explicit dynamic analysis, then an implicit static analysis is performed to simulate the complete process [22]. This new method is able to successfully simulate the entire process from the dynamic response due to laser shock pressure to the final stable state after the elastic strain energy is released [23]. The finite element simulation algorithm can be divided into two major steps, as schematically shown in Fig. 14

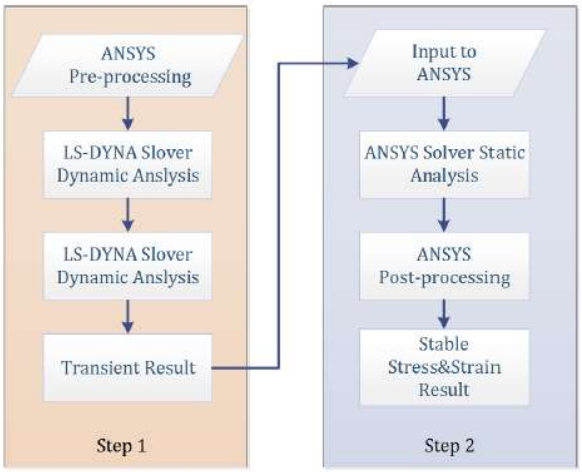

Fig. 14 – FEM logic flow chart, adopted with permission from [4]

The explicit analysis is first applied to simulate the transient response during the interaction between the laser pulse and the target material. The plasma-induced shockwave pressure is simulated by the ANSYS/LS-DYNA explicit solver. Transient results such as the stress/strain field and the deformed geometry are obtained from the dynamic analysis in step 1. Those results are subsequently used as the initial conditions to perform the simulation in step 2. The objective of the second step is to obtain the residual stress field distribution in the target material. This objective is achieved with the help of ANSYS implicit solver as a static analysis. To simplify the model, single pulse assumption is applied during the entire simulation process. Likewise, prior to the experimental process, the FE model is first explored to predict how the metal thickness could influence the concave/convex bending. Afterwards, the FE model is applied to study the effect of the laser pulse energy on the forming mechanism.

The setup of FE model is shown in Fig. 15, where only a quarter of the system is considered to save computational costs. The red-highlighted region shows the elements

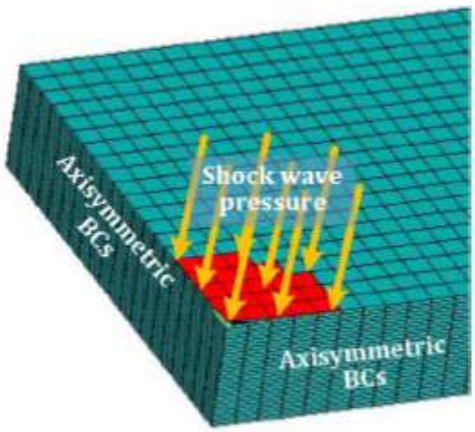

Fig. 15 – FEA Simulation Configuration, Adopted with Permission from [4]

where laser-induced shockwave pressure is applied. Symmetric boundary conditions are applied on the two cross-sections bisecting the center of the sample, and the highlighted area is approximately a quarter of the whole beam size. The shockwave peak pressure is predicted from Fabbro's model [14], $P_0 = 0.01\sqrt{\frac{\alpha Z I_0}{2\alpha+3}}$, where α is the ratio of internal energy transferred to thermal energy, Z is the effective impedance coefficient for the confinement-target system, and I_0 is the peak intensity of the laser beam, which can be written as $I_0 = \frac{4E}{\pi\tau \ ^2}$, where E is the single pulse energy, τ is the pulse duration and D is the spot size, respectively. The simulation results for the entire cross-section are obtained by mirroring the result of this one-quarter setup in the post-processor of ANSYS.

4.2.2 Simulation Results

Fig. 16 shows the bending deformation for different choices of sheet metal thickness [4]. There is a close correlation between the thickness and the bending angle. With the increase of sample thickness, the bending angles decrease for all the cases. The concave/convex

bending transitions when the specimen thickness reaches 0.9 mm. The simulation result is consistent with experimental results, validating that the concave/convex bending deformation switches at a certain thickness for a specific sheet metal.

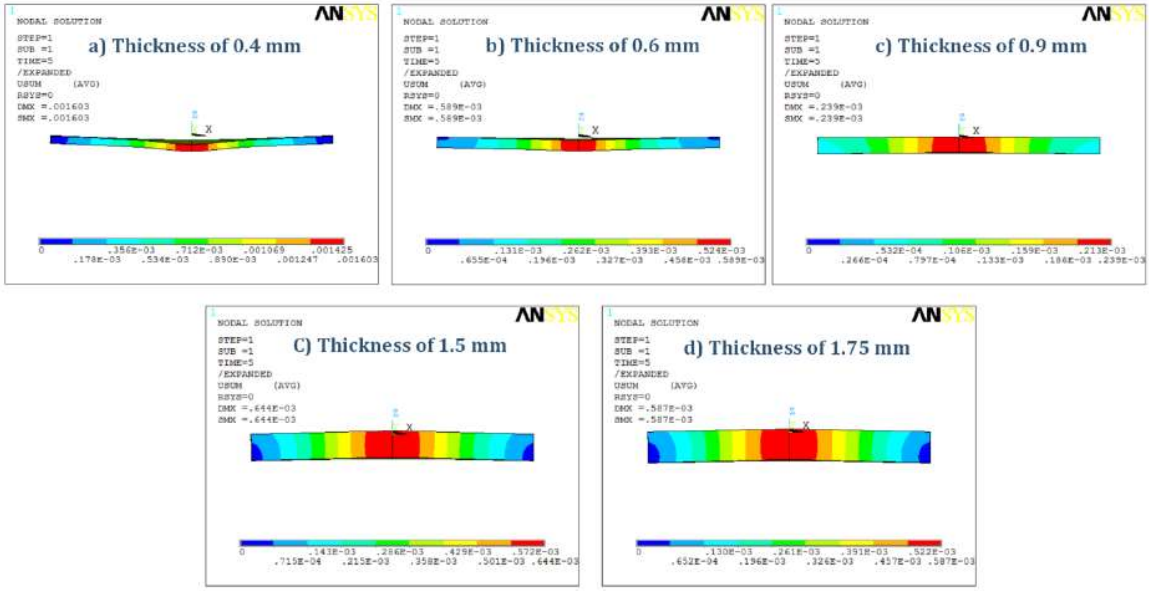

Fig. 16 - Simulation results of bending deformations for different thickness of sheet metal, adopted with permission from [4]

Fig. 17 shows the influence of different laser pulse energies on the bending direction by applying the FE model [4]. The thickness of the substrate is fixed to be 0.6 mm and pulse energy is set to be (a) 0.2 J, (b) 0.3 J, (c) 0.4 J and (d) 0.6 J. Fig 17 (a, b) show the convex deformation and Fig 17 (c, d) show the concave deformation. For a fixed thickness, with the increase of pulse energy, the bending deformation transitions from convex to concave, which is consistent to the experimental results. Therefore, the results in Fig. 16 and Fig. 17 show that under a given laser pulse energy, there is a threshold thickness where the deformation behavior switches from concave to convex. The sample will bend in the convex direction when the thickness is greater than the threshold thickness, and will bend

concavely when the thickness is less than the threshold thickness. The bending shape of two forming mechanisms is determined by the depth of residual stress.

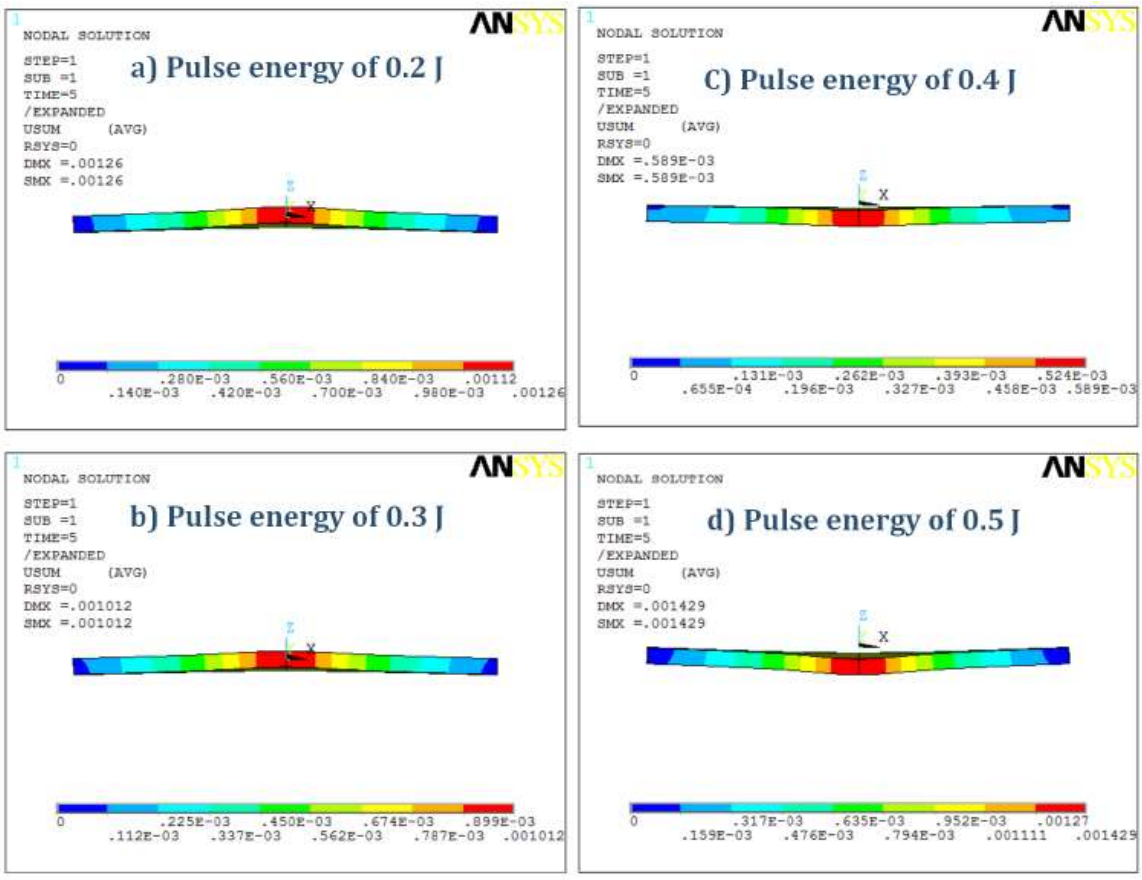

Fig. 17 - Simulated deformation of different pulse energies, adopted with permission from [4]

5. Alternative Methods

5.1 Femtosecond Laser Peen Forming

Sagisaka, et al [3, 9, 24] demonstrated the largest benefits of femtosecond LPF are its ability to eliminate the need for ablative coatings and confinement media, and provide weaker shock waves than nano-second LPF, resulting in convex curvature of thin work pieces. Due to the relatively long pulse width of a nano-second laser, it is difficult to produce weak shock waves in a thin sample. This presents a problem for convex bending of thin sheet metals. Mode IV, concave bending, usually occurs under these conditions, unless dampened by an ablative layer sufficient of absorbing the shock to limit the penetration depth of the compressive residual stresses. Within the femtosecond regime, low energy, coupled with short pulse durations allow for minimal shockwave pressures induced to the sample, thus enabling convex curvature on very thin materials, without the need for ablative and confinement media. In fact, in femtosecond LPF, the use of confinement media has an adverse effect on the process. Pulsed femtosecond laser irradiances are absorbed by water, significantly reducing the energy at the surface of the material. This decreases the amount of equipment required to processes the sheet metal. Conversely, however, irradiance values of femtosecond lasers are too small to produce concave bending in thick plates that nano-second lasers are capable of bending.

Their investigations sought relationships between fluence, bend angle and direction, effect of irradiated pulse density, overall shape, and influence of laser stability for Pure Aluminum, Phosphor Bronze and Stainless Steel. It was found that high fluence and high irradiated pulse density decreased bending radius of sheet metals. Several complicated

shapes were achieved simply by changing the fluence and scanning path. In addition, they discovered that the bending efficiency of a material is related to the stress flow. This shows that LPF is based on the mechanical effects of the laser-material interaction, and softer material is easier to bend using these methods.

5.2 Heat Assisted Nano-Second Laser Peen Forming

Hu, et al. [25] proposed a method to bend high strength titanium with laser-assisted local heating. A CW Fiber laser used to heat the bottom surface was applied coaxially with the pulsed laser used for inducing the shockwave. The CW heating laser and pulsing laser

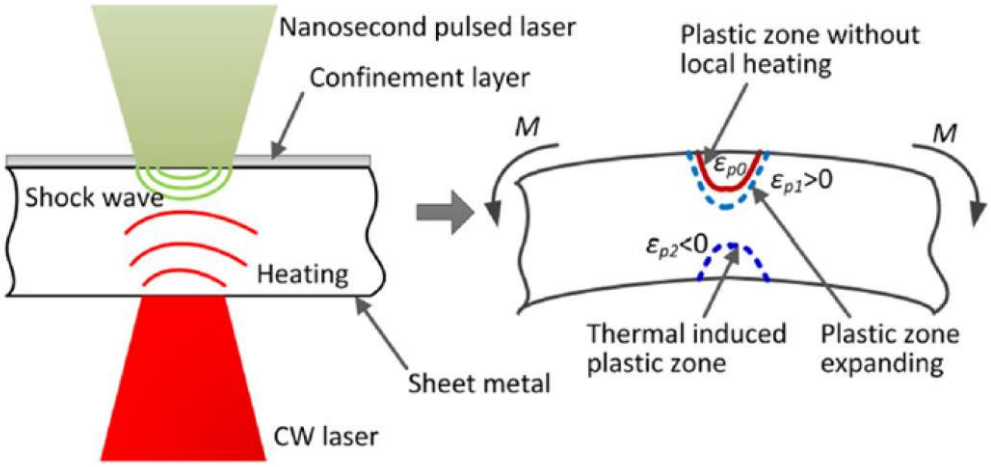

Fig. 18 - Laser-assisted local heating LPF, adopted with permission from [25]

moved in sync with one another to produce a scanned area. The process setup was like traditional LPF methods except the use of an ablative coating. Fig. 18 illustrates the setup and the thermally induced plastic zone that is generated when the CW heating laser is applied. Because the strength of materials like titanium are sensitive to temperature, deformation resistance within the shocked zone is reduced, and plastic deformation of the

laser peened area is much easier to achieve. An important discovery during these trials was the use of silicone oil as a confinement media does not provide the essential properties required during the LPF process. Due to the high viscosity of silicone oil and high-speed processing of LPF, the slow flow of silicone oil cannot replenish the laser peening site with confining media in time to provide confinement for the subsequent laser pulse. Thus, water is used, and heating of the sample is applied on the bottom side of the sample to avoid excessive evaporation of the confinement media.

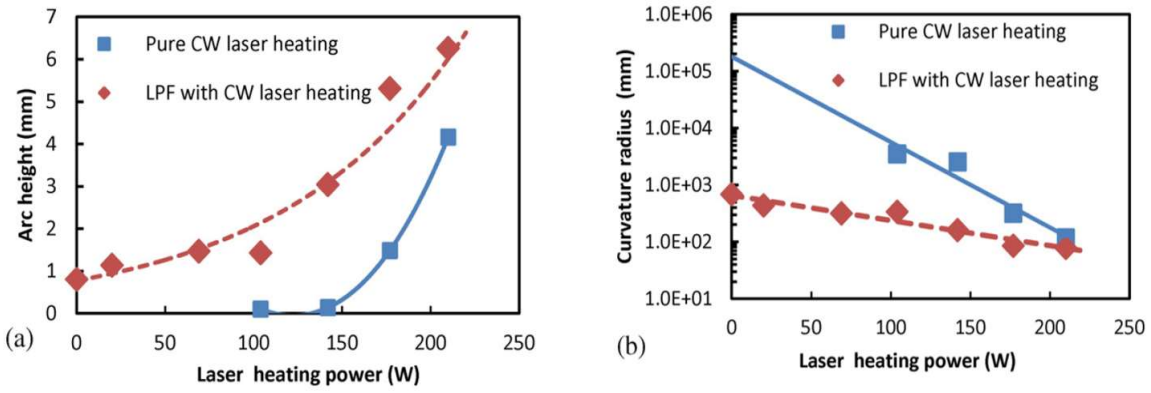

Fig. 19 – Effect of laser assisted local heating LPF on (a) Arc height and (b) Curvature radius, adopted with permission from [25]

In the thermal bending regime, three mechanisms can contribute to the overall shape of the sample [13]. Of the three thermal mechanisms in laser forming, the temperature gradient mechanism dominates the thermal mechanism that contributes to the final shape of the material in heat assisted laser peen forming. Fig. 19 demonstrates how the laser-assisted local heating benefits the LPF process for the experiments conducted by [25]. By investigating bending deformation and microstructural changes using numerous laser heating powers, it was proven that heat assisted LPF by laser-assisted local heating was an effective method for improving the formability of titanium by increasing the depth of

plastic deformation during processing. The bend radius was also decreased when compared to traditional LPF methods. The experiments conclude that this approach is beneficial for convex bending because laser heating of the bottom surface generates an elevated temperature on the top surface, decreasing the materials resistance to plastic deformation at the incident beam site. Additionally, it was shown that an increase in laser power heating leads to a decrease in bending radius due to the materials increased capability to deform plastically at the laser induced shock region.

6. Conclusion

Recent developments in LPF research and related techniques have been reviewed with an emphasis on summarizing the process design, consideration of processing parameters, mechanisms of forming behavior, laser-material interactions, simulation approaches, and alternative LPF methods. The forming mechanisms contributing to the net bending angle are explored individually by describing the response of the system to applied stimuli and constraints. Two models of laser-material interaction describing the physical process have been discussed and their application to the LPF process has been warranted. In addition, factors in recent developments of similar LPF processes using ultra-short lasing systems have been reflected on.

To utilize LPF in the manufacturing industry, understanding how all the laser parameters, forming mechanisms, and physical processes of the formed shape relate to each other, and modeling their relationships to one another, is critical to accurately control the bending angle of the work piece. From the several investigations that were reviewed, a fundamental understanding of the bending mechanisms, principles of laser-material interactions, simulation and modeling techniques for FEA investigations, and how each processing parameter influences the results, has been described.

CHAPTER II

7. Laser Peen Forming without Ablative Coating and Confining Media

7.1 Background and Motivation

The complexities associated with traditional LPF processing lead to excessive cost and set up times. Special equipment to maintain a confining media is required, and processing must be temporarily ceased to apply ablative coatings for subsequent processing in multiple pass operations. Additionally, optical systems used in LPF must be protected from process equipment activated contamination, such as water splashing on the focusing lens and mirrors. Furthermore, in-service LPF processing of engineering components is difficult to access and requires long equipment down time. This introduces a significant hindrance to process efficiency for industrial applications.

It is hypothesized that a novel low-cost and simplified LPF process design without ablative coating and confining media can result in desired bending behavior of metallic thin foils. It is expected that such a new process design will enable the practical applications of LPF for industrial purposes. In this study, we develop the LPF process without ablative coating and confining media. A series of experiments were conducted to investigate the feasibility of the newly proposed processing of metallic thin foils.

7.2 Experiment

7.2.1 LPF without ablative coating and confinement

LPF without ablative coating and confinement setup is similar to standard LPF experiment setups. Fig. 20 illustrates the optical system arrangement, mounting provisions for the sample assembly, and position control via X-Y stages. A Q-Switched Nd:YAG nanosecond pulsed laser systems operating at 1,064 nm wavelength provides the necessary laser requirements for an LPF experiment. The cantilevered sample and stage assembly

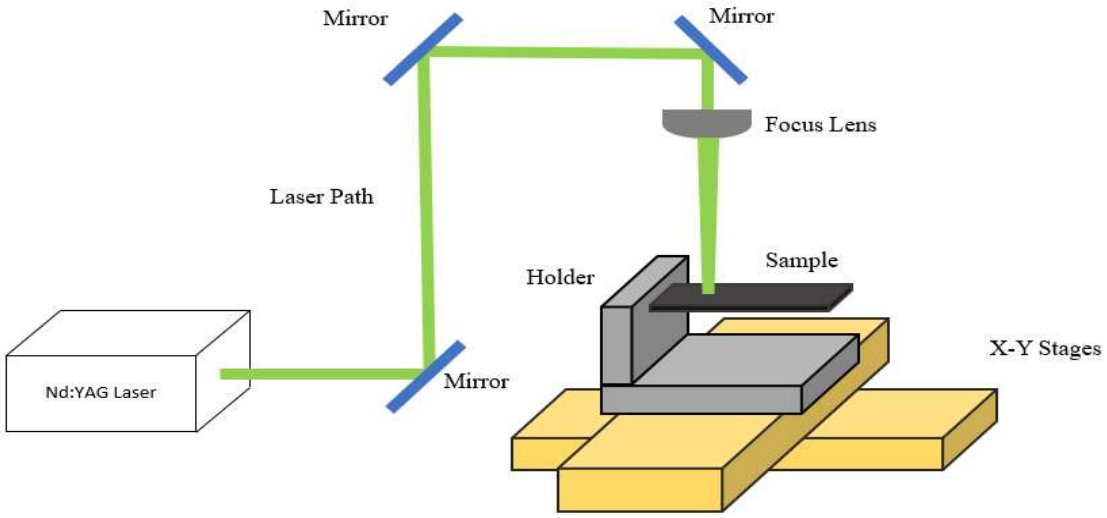

Fig. 20 – Schematic of LPF experimental setup without ablative coating and confinement

rests atop two stages. Each stage is oriented 90^{o} relative to one another, providing planar motion of the sample, normal to the direction of the incident beam. The laser beam is directed to the target through a series of reflecting mirrors and a convergent lens. When a high-intensity pulse is injected to the sample surface it is instantaneously vaporized, then ionized [3, 8, 9], which forms a high pressure, rapidly expanding plasma. As a result, a shockwave is induced due to the ultrafast expansion of plasma.

Three metallic thin foil materials were selected for the experimental study, including, Aluminum Alloy 1100 with a thickness of 0.254 mm, Stainless Steel 304 with a thickness

of 0.0508 mm, and Aluminum Alloy 6061-T6 with a thickness of .508 mm. All samples were cut to 10 mm in width and were cantilevered out by 10 mm in length. The first scanning line was introduced 8.4 mm from the cantilevered edge of the sample piece. Each experiment was repeated 3 times to validate consistency in experimental data. The laser parameters for all experiments are given in Table 1.

Table 1. Laser parameters for LPF without ablative coating and confining media

Laser Parameter	Value
Spot Diameter	1.5 mm
Pulse Width	5 ns
Pulse Frequency	10 Hz
Wavelength	1,064 nm
OR	53%

The first investigation studied the effect of the number of passes on the bend angle for a low and high laser intensity, relative to traditional LPF laser fluences, on a given material. Experimental parameters for this investigation are given in Table 2.

Table 2. Experiment details for study on effect of number of passes on bend angle

Parameter	Experiment 1	Experiment 2
Laser Intensity	0.6 GW/cm^2	3.6 GW/cm^2
Number of Passes	5, 10, 15, 20	5, 10, 15, 20
Material	AA 1100	AA 1100

The second investigation studied the effect of varying laser intensities on the bend angle for various materials with a preset number of passes. The experimental parameters for this investigation are given in Table 3.

Table 3. Experiment details for study on effect of laser intensity on bend angle

Parameter	Experiment 1	Experiment 2	Experiment 3
Laser Intensity	0.6, 1.2, 2.4, 3.6 GW/cm^2	0.6, 1.2, 2.4, 3.6 GW/cm^2	0.6, 1.2, 2.4, 3.6 GW/cm^2
Number of Passes	5	5	5
Material	AA 1100	SS 304	AL 6061-T6
Thickness	0.254 mm	0.0508 mm	0.508 mm

7.2.2 Characterization and Measurement

LPF processing of engineering metals can produce a variety of bend angles, ranging from large to very small – in some cases as small as the minute, and even second scale – given the appropriate laser/material parameters during an experiment. As such, suitable equipment capable of measuring small deformations is required to accurately detect bending below 10°. For the experimental studies described above, a laser displacement sensor (micro-epsilon optoNCDT ILD1401-10) with a static resolution of 1 µm directed at the top surface of the cantilevered end of a sample piece detects the vertical location of the

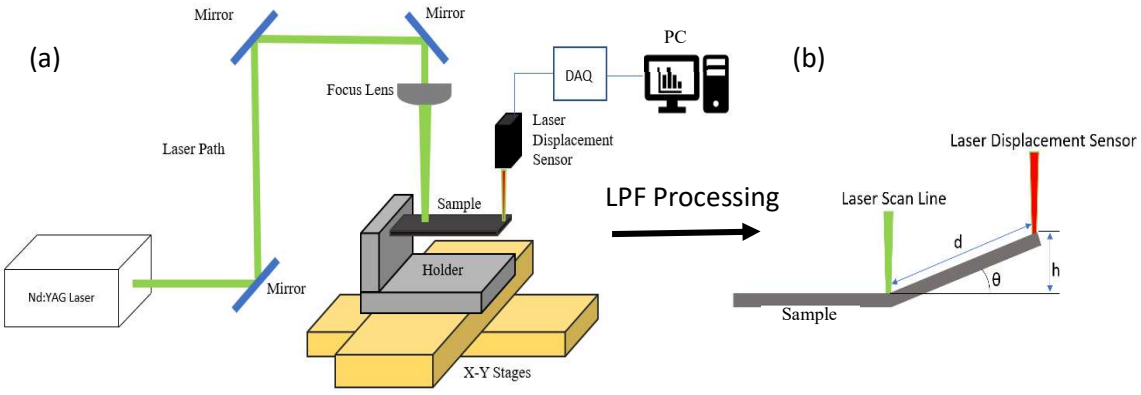

Fig. 21 – Schematic of (a) Bending detection equipment and (b) Geometry model used to calculate bending for angles less than 10°

end of the sample, as illustrated in Fig. 21 (a). A signal is sent to a Data Acquisition unit (National Instruments myDAQ) that converts the signal from the laser displacement sensor into a current, in mA, that is displayed by LabView on the computer screen. The current is used to calculate the distance of the surface of the sample piece from the bottom edge of the laser displacement sensor, providing an initial position of the sample piece prior to LPF processing. After LPF processing of the work piece, the laser displacement sensor reading is recorded again, and the change in height of the end of the beam, h, is recorded at a distance, d, from the clamped end, as shown in Fig. 21 (b). This information is used to calculate the final bend angle, θ, according to the geometry shown in Fig. 21 (b). For angles greater than 10°, an angle finder was utilized to accurately measure the bend angle, taking in to consideration the bend radius of the sample piece that the laser displacement sensor cannot account for according to this geometry model.

To understand the effect that processing without ablative coatings has on the surface of a sample, a random sample of AA 1100 were selected and placed under an optical microscope. Fig. 22 (a) and (b) show unprocessed and processed samples under a USB digital microscope (Crenova model UM012C) with 20x magnification to show processing details such as processing tracks and overlapping ratio. Fig. 22 (c) and (d) illustrate unprocessed and processed samples under an optical microscope (Leica model dm 2700 m) with 50x magnification to show surface details of a single processing track. The samples were then put in to a profilometer to obtain before and after surface roughness properties. The unprocessed sample had a roughness of $R_a = 0.575 \pm 0.10$ μ. The process samples of experiment 1 and 2 were both exposed to 20 passes. Sample 1 (using a laser intensity of

0.6 GW/cm2) had an average roughness value of $S_a = 3.33 \pm 0.48$ µm, and sample 2 (using a laser intensity of 3.6 GW/cm^2) had an average roughness of $S_a = 1.82 \pm$ µm

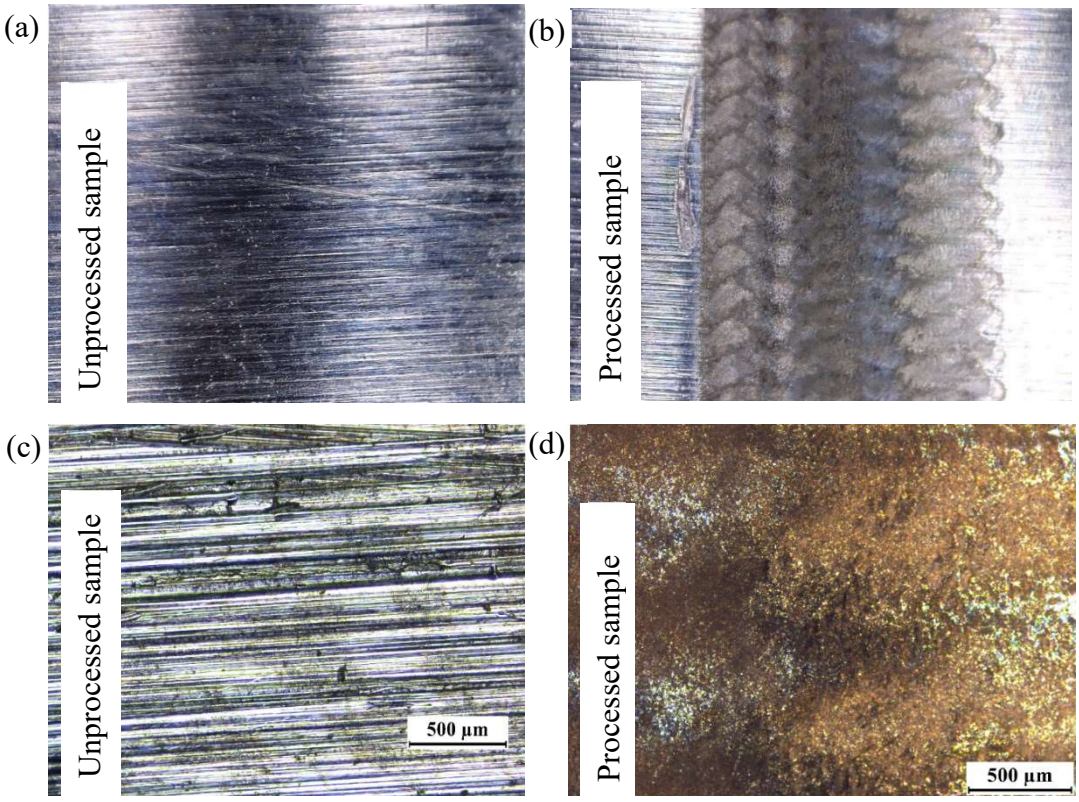

Fig. 22 – Samples of AA 1100 at 20x magnification for (a) pre-processing, and (b) post-processing, and 50x magnification for (c) pre-processing, and (d) post-processing

7.3 Experimental Results and Discussion

The number passes, or number of times the sample surface is processed, has a significant effect on the cumulative bend angle of the sample piece. Fig. 23 (a) and (b) summarize the experimental studies investigating this effect for 0.254 mm thick Aluminum Alloy 1100 exposed to laser intensities of 0.6 GW/cm^2 and 3.6 GW/cm^2, respectively, and an OR of 53% and number of tracks equal to 4. It is found that the bending angle accumulates by increasing the number of passes. For a sample being processed by a 0.6

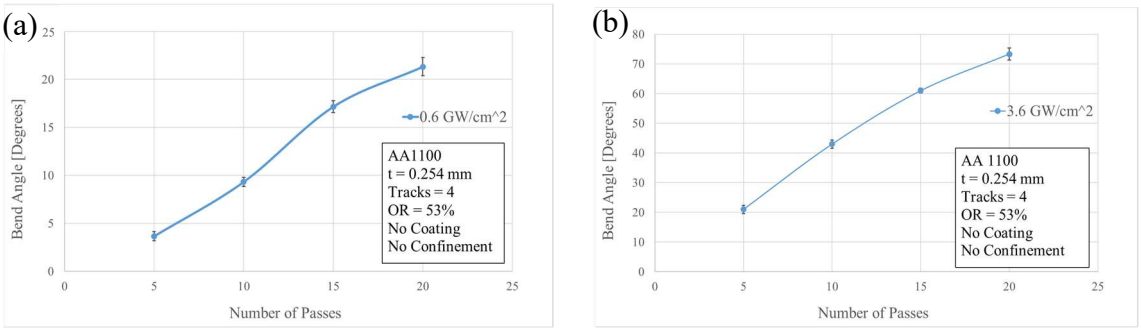

Fig. 23 – Effect of number of passes on bending angle of AA 1100 for laser intensities of (a) 0.6 GW/cm^2 and (b) 3.6 GW/cm^2

GW/cm^2 laser intensity, the concave bending angle is increased from 3.67° to 21.33° by increasing the number passes from 5 to 20, in 5 pass intervals. The average standard deviation for all 4 data points among the 3 series of tests is 0.63°. When the laser intensity is increased to 3.6 GW/cm^2, given the same laser processing parameters, the concave bending angle increases by 52.33° from 21° to 73.33°. The average standard deviation for all 4 data points among these 3 series of tests is 1.42°. As indicated by Fig. 23, the number of passes affects the accrued bending angle, however, has no effect on the bending mode.

The laser intensity is a significant parameter in LPF processing, contributing to both direction and magnitude of the bending angle. It can be deduced from Fig. 24 that, for a given laser intensity, an increase in material thickness is associated with a decrease in bending angle. For this series experiments, the material thickness remained under the critical thickness threshold, and therefore the mode of bending remained concave throughout the study. As shown in Fig. 24 (a), for AA 1100, the bending angle increases with an increasing laser intensity. For a sample 0.254 mm thick, with an OR or 53%, number of tracks equal to 4, and 5 passes, the bend angle is increased from 4° to 20.5° by increasing the laser intensity from 0.6 GW/cm^2 to 3.6 GW/cm^2. The average standard

deviation for all 4 data points among these 3 series of tests is 0.90°. Similarly, with the same given laser processing parameters, as shown in Fig. 24 (b), a 0.0508 mm thick sample of 304 SS rapidly increases from 87.66° to 90° as the laser intensity increases from 0.6 GW/cm^2 to 3.6 GW/cm^2. The average standard deviation for all 4 data points among the 3 series of tests is 0.24°. Finally, using the same laser parameters, as shown in Fig. 24 (c), a 0.508 mm thick sample of AA 6061-T6 increases sligthly by 0.17° from 0.24° to 0.41° as

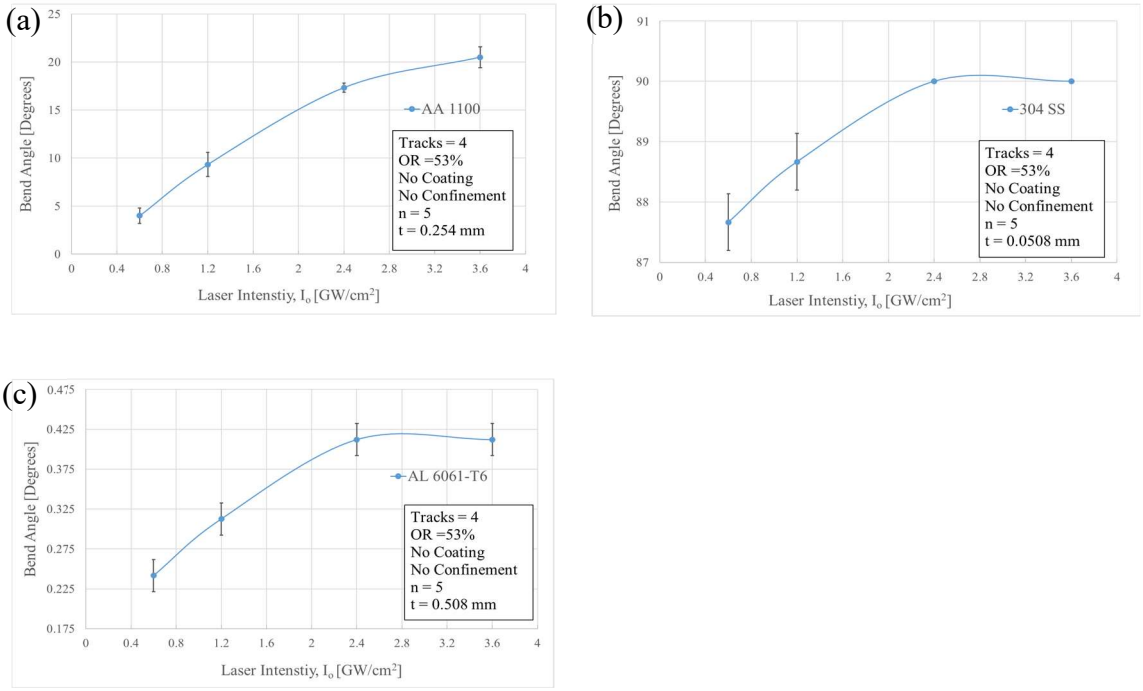

Fig. 24 – Effect laser intensity on bending angle of (a) AA 1100 (b) SS 304 and (c) AA 6061-T6

the laser intensity moves from 0.6 GW/cm^2 to 3.6 GW/cm^2. The average standard deviation for all 4 data points among the 3 series of tests is 0.02°

As indicated by Fig. 24, the increase in laser intensity has a significant impact on the overall bend angle. However, if the laser intensity increases too much, significant material

damage will be incurred, and, therefore, allowable laser intensity is limited. As such, the sample thickness governs both the direction and amplitude of the bending angle, particularly for concave bending. Very thin materials bend to 90° with ease, as demonstrated. However, as the material thickness increases past the critical thickness threshold, the effects of the shockwave induces residual stress diminishes to a point that 90° convex bending is not possible, and thus LPF is limited by the thickness of the sample piece.

In order to demonstrate the lost affect of ablative materials *not* under confinement, a test was conducted to compare a 0.254 mm thick sample of AA 1100 with no ablative coating and one with black tape ablative coating. Fig. 25 demonstrates the significant difference by elucidating that the bend angle without the coating after 5 passes, using 4 tracks, and an OR of 53%, is 17.44°, and with a black tape ablative coating, is 1.98°. It is

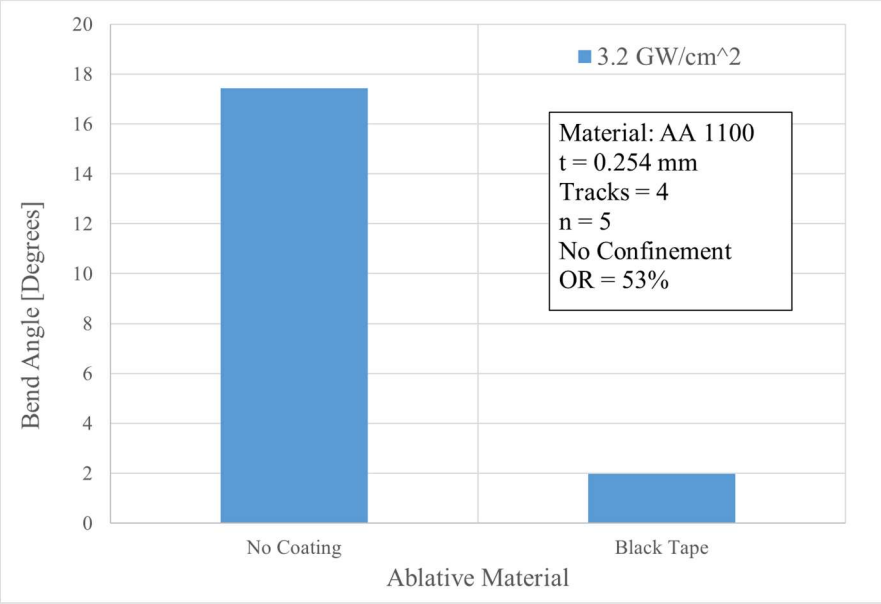

Fig. 25 – Comparison of 0.254 mm thick AA 1100 with and without ablative coating

therefore counterproductive to employ a black tape ablative coating to an LPF process not under confinement.

8. Conclusion

In this study, LPF without ablative coating and confining media was carried out on various metallic thin foils. The effects of laser scanning number and laser intensity on the bending angle were investigated. The surface profile of laser-processed area was characterized with a focus on surface roughness. It was found that the process efficiency of LPF without ablative coating and confining media is strongly affected by the thickness and strength level of the workpiece materials. Furthermore, LPF without ablative coating results in a larger bending angle as compared to the sample processed by LPF with ablative coating. This is attributed to the energy loss when the laser-induced shockwave propagates through the ablative coating material. However, LPF without ablative coating leads to an increase in the surface roughness due to the direct interaction between laser beam and workpiece materials. It is envisioned that such a novel low-cost and simplified LPF process design without ablative coating and confining media can effectively bend metallic thin foils and become prevalent to widespread industrial applications. In future work, a systematic study of this new LPF process by an integrated experimental and FEM simulation effort is needed for process optimization and control. In addition, an investigation on the bending response of magnesium AZ31B to LPF processing could overcome its vulnerability to cracking during forming.

References

[1] L. Hackel, F. Harris, Contour forming of metals by laser peening, Google Patents, 2002.
[2] C. Pence, H. Ding, N. Shen, H. Ding, Experimental analysis of sheet metal micro-bending using a nanosecond-pulsed laser, The International Journal of Advanced Manufacturing Technology 69(1-4) (2013) 319-327.
[3] Y. Sagisaka, M. Kamiya, M. Matsuda, Y. Ohta, Application of Femtosecond Laser Peen Forming to Sheet Metal Bending, J Laser Micro Nanoen 7(2) (2012) 158-163.
[4] H. Ding, N. Shen, K. Li, W. Bo, C.N. Pence, H. Ding, Experimental and Numerical Analysis of Laser Peen Forming Mechanisms of Sheet Metal, (2014) V002T02A102.
[5] H. Shen, J. Hu, Z. Yao, Analysis and control of edge effects in laser bending, Optics and Lasers in Engineering 48(3) (2010) 305-315.
[6] M. Zhou, Y.K. Zhang, L. Cai, Laser shock forming on coated metal sheets characterized by ultrahigh-strain-rate plastic deformation, Journal of Applied Physics 91(8) (2002) 5501-5503.
[7] Y. Hu, X. Xu, Z. Yao, J. Hu, Laser peen forming induced two way bending of thin sheet metals and its mechanisms, Journal of Applied Physics 108(7) (2010) 073117.
[8] B.X. Wu, Y.C. Shin, A one-dimensional hydrodynamic model for pressures induced near the coating-water interface during laser shock peening, Journal of Applied Physics 101(2) (2007).
[9] Y. Sagisaka, K. Yamashita, W. Yanagihara, H. Ueta, Microparts processing using laser cutting and ultra-short-pulse laser peen forming, Journal of Materials Processing Technology 219 (2015) 230-236.
[10] S.T. K. Kondo, A. Kato, Investigations on Peen Forming. II.--Forming Mechanism, First International Conference on Shot Peening: Paris 14-17 (1981) 565-581.
[11] J. Johnson, R. Rohde, Dynamic Deformation Twinning in Shock-Loaded Iron, Journal of Applied Physics 42(11) (1971) 4171-4182.
[12] Y. Hu, Y. Han, Z. Yao, J. Hu, Three-Dimensional Numerical Simulation and Experimental Study of Sheet Metal Bending by Laser Peen Forming, Journal of Manufacturing Science and Engineering 132(6) (2010) 061001.
[13] H. Shen, F. Vollertsen, Modelling of laser forming – An review, Computational Materials Science 46(4) (2009) 834-840.
[14] R. Fabbro, J. Fournier, P. Ballard, D. Devaux, J. Virmont, Physical Study of Laser-Produced Plasma in Confined Geometry, Journal of Applied Physics 68(2) (1990) 775-784.
[15] D. Devaux, R. Fabbro, L. Tollier, E. Bartnicki, Generation of Shock-Waves by Laser-Induced Plasma in Confined Geometry, Journal of Applied Physics 74(4) (1993) 2268-2273.
[16] D. Devaux, R. Fabbro, J. Virmont, Generation of Shock-Waves by Laser-Matter Interaction in Confined Geometries, J Phys Iv 1(C7) (1991) 179-182.
[17] J.D. Okeefe, C.H. Skeen, Laser-Induced Stress-Wave and Impulse Augmentation, Appl Phys Lett 21(10) (1972) 464-&.
[18] L.C. Yang, Stress Waves Generated in Thin Metallic-Films by a Q-Switched Ruby-Laser, Journal of Applied Physics 45(6) (1974) 2601-2608.
[19] N.C. Anderholm, Laser Generated Pressure Waves, B Am Phys Soc 13(3) (1968) 388-+.
[20] N.C. Anderholm, R.R. Boade, Laser-Induced Stress Waves in Quartz Phenolic, Journal of Applied Physics 43(2) (1972) 434-+.
[21] N.C. Anderholm, Fast Gas Switch for Characterizing Laser Output Pulses, Appl Optics 11(9) (1972) 2057-+.
[22] Y.X. Hu, Z.Q. Yao, Overlapping rate effect on laser shock processing of 1045 steel by small spots with Nd : YAG pulsed laser, Surf Coat Tech 202(8) (2008) 1517-1525.

[23] J.L. Ocaña, M. Morales, C. Molpeceres, O. García, J.A. Porro, J.J. García-Ballesteros, Short pulse laser microforming of thin metal sheets for MEMS manufacturing, Applied Surface Science 254(4) (2007) 997-1001.
[24] Y. Sagisaka, M. Kamiya, M. Matsuda, Y. Ohta, Thin-sheet-metal bending by laser peen forming with femtosecond laser, Journal of Materials Processing Technology 210(15) (2010) 2304-2309.
[25] Y. Hu, M. Luo, Z. Yao, Increasing the capability of laser peen forming to bend titanium alloy sheets with laser-assisted local heating, Materials & Design 90 (2016) 364-372.
[26] J. L. Ocaña, M. Morales, J. García-Ballesteros, J. Porro, O. García, C. Molpeceres, Laser shock microforming of thin metal sheets, Applied Surface Science, vol. 255, no. 10 (2009) 5633-5636.